Nucleation, aggregation, annealing, and disintegration of granular clusters

Jorge González-Gutiérrez,[1] J. L. Carrillo-Estrada,[1] and J. C. Ruiz-Suárez[2]
[1]*Instituto de Física, Benemérita Universidad Autónoma de Puebla, A. P. J-48, Puebla 72570, México*
[2]*CINVESTAV-Monterrey, PIIT, Nuevo León, 66600, México*
(Received 4 November 2013; published 9 May 2014)

The processes of nucleation, aggregation, annealing, and disintegration of clusters of non-Brownian paramagnetic beads in a vibrofluidized system are experimentally investigated. The interaction among the beads is induced by a magnetic seed composed of two dipoles allocated outside the container cell. We observe a clearly differentiated nucleation stage, whose evolution (nucleation time versus acceleration strength) follows a power law. Thereafter, the beads aggregate forming 2D disordered clusters around the nucleus. Both processes (nucleation and aggregation) are determined by the competition between magnetic forces and the drag produced by a thermal bath created by glass particles. Once the agglomerates reach a final state (shape and length), they are annealed by increasing and decreasing the granular temperature. We found that the fractal dimension and the lacunarity index clearly describe the structural variations of the clusters. Our discussion on this phenomenon is addressed, making a rough analogy with the glass transition in a super-cooled liquid. Finally, we study the disintegration of the clusters as a function of time and the density of the surrounding gas. The question is not if, but how they disintegrate upon removing the external field; we find that the disintegration follows an exponential decay.

DOI: 10.1103/PhysRevE.89.052205 PACS number(s): 45.70.Qj, 64.60.Q−

I. INTRODUCTION

Nucleation and aggregation are very frequent phenomena in nature; for example, atmospheric aerosol nucleation [1], colloid crystallization [2], bubble formation [3], colloidal aggregation in microgravity [4], vesiculation of membrane proteins [5], and meteorite formation [6]. In most of the cases, the structures are disordered with fractal or mutifractal characteristics [7–14].

Annealing is a process by which a solid structure is reordered. Typically, this process involves a temperature increment followed by a slow cooling [15,16]. This has been applied to many physical systems: ferroic materials [17], spin glasses [18], liquid crystals [19], and even where the effective temperature is defined in terms of the dominant physical variables, instead of the thermodynamic temperature [20].

Some studies on the dynamics of nucleation and crystallization [21,22], aggregation [23–25], and annealing [26], in vibrofluidized granular systems of hard spheres have been reported, as well as similar studies using soft (interacting) particles [27–32].

In this paper, we revisit this subject carrying out an experimental study of the nucleation, aggregation, and annealing processes of clusters composed by non-Brownian paramagnetic particles in a vibrofluidized granular system. Our aim is to understand how the competition among the inertial forces due to the vibration, the drag produced by the glass and steel particles, and ultimately the magnetic forces, drives the dynamics of the system.

II. EXPERIMENTAL DETAILS

We perform our experiments in a transparent acrylic three-dimensional cell (15 × 15 × 3 cm), attached to a vibrator that produces vertical shakes; see Fig. 1(a). We use steel spheres with diameter $r_0 = 1.61$ mm and mass of 0.017 g, and glass particles with diameter $d = 2$ mm and mass of 0.0074 g. The glass beads are used to introduce additional stochasticity into the system. Also, they act as a thermal bath to ensure that as the steel particles condense or aggregate, the effective temperature of the system does not go to zero. The concentration rate, ϕ, is defined as the ratio between the number of metallic particles n_p and the number of glass particles n_g. To induce an interaction among the steel beads in the system, we used two magnetic spheres that we allocate at the rear part of the bottom cell. The strength of the magnetic dipoles is $M = 12$ kG, with a separation of $l = 20$ mm. The magnetic moments are set perpendicular to the base and oriented opposite to each other; see Fig. 1(b). Henceforth, we would refer to both dipoles as the seed.

Image data are acquired using either a high-speed digital camera (DRS Lightning RDT Plus) at 100 fps, or a slow one (Pixelink PL - B742V) at 1 fps, as shown in Fig. 1(a). Depending on the speed of the process recorded we use one or the other.

Following P. M. Reis *et al.* [33], the granular temperature is defined as: $T_g = \frac{1}{2}(\langle v_x^2\rangle + \langle v_y^2\rangle)$, where v_x and v_y are the components of the velocity in the 2D plane. Here the brackets $\langle . \rangle$ denote a time average. T_g is proportional to $\Gamma = A\omega^2/g$ for small intervals [27,33,34], where A and ω are the amplitude and angular frequency given by the shaker and g is the acceleration due to gravity.

III. NUCLEATION AND AGGREGATION

We begin our experiments keeping the system fluidized at some specific values of Γ and ϕ. The particles inside the cell move in a random walk homogeneously dispersed, until the magnetic dipoles are suddenly attached under the base. The seed induces dipole moments in the paramagnetic particles so they interact. If this magnetic interaction overcomes the inertial and drag forces, the particles attach to each other. It could be perhaps of some interest for the reader to know that the magnetic pair interaction between any two particles may

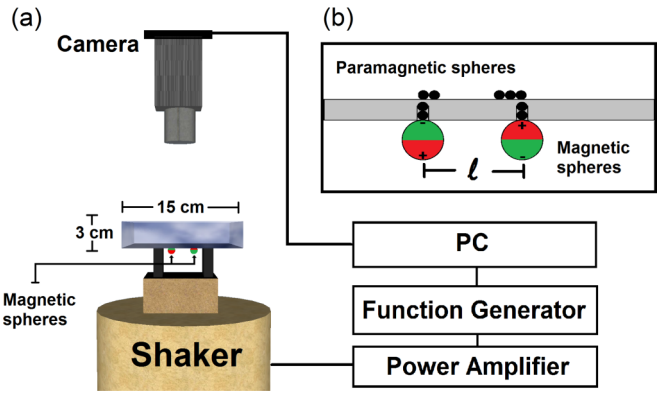

FIG. 1. (Color online) (a) A schematic diagram of the experimental apparatus. Image data are obtained from the top by a digital camera. (b) A zoom of the zone where two neodymium magnetized spheres are located underneath the base of the cell. These spheres have 5 mm of diameter with a magnetization of 12 kG. Note that the magnetization of each sphere is transmitted through the bottom of the cell with two paramagnetic small beads embedded in the acrylic base.

be approximately given by the interaction between two point dipoles [27],

$$U_{i,j} = \frac{\mu^2}{r_{ij}^3}[\hat{\mu}_i \cdot \hat{\mu}_j - 3(\hat{\mu}_i \cdot \hat{r}_{ij})(\hat{\mu}_j \cdot \hat{r}_{ij})], \qquad (1)$$

where μ is the magnitude of the dipoles, $r_{ij} = |\mathbf{r}_j - \mathbf{r}_i|$ is the separation distance, $\hat{\mu}_i$ and $\hat{\mu}_j$ and $\hat{r}_{ij}$ are, respectively, unit vectors in the direction of the dipole moments and in the direction of the line between them.

Due to the magnetic interaction the nucleation starts. This consists of a slow formation of a chain of paramagnetic particles linking both poles of the seed [see Fig. 2(a)]. Invariably, it is observed that the paramagnetic particles adhere to any site of the initial chain linking the two dipoles. How fast the linear nucleus grows depends on the competition between the magnetic interaction, which favors the chain growth, and the inertial and drag interactions produced by the vibration of the cell and the collisions with the glass particles. The aggregation becomes energetically favorable only when a chain connects the two poles of the seed. One may use the classical nucleation theory to describe qualitatively the nucleation and aggregation process. In such theory the formation and size of a nucleus is explained by the change of the free energy. This is produced by the competition of a bulk and a surface energy. The former gives a negative contribution and the latter a positive one. It is only when a cluster reaches a critical size, when the bulk contribution surpasses that of the surface and then the nucleus becomes stable. This conceptual frame has been used to describe biopolymer's nucleation and aggregation [35] and nucleation and crystallization of hard sphere colloids [2].

In the granular system studied here, the nucleation and aggregation phenomena, as seen in Fig. 2(a), cannot be treated using the classical nucleation theory. Nevertheless, given some similarities we can lay down the following heuristics: The growth of the 2D clusters is also a competition between two processes that finally induces a reduction of free energy. On

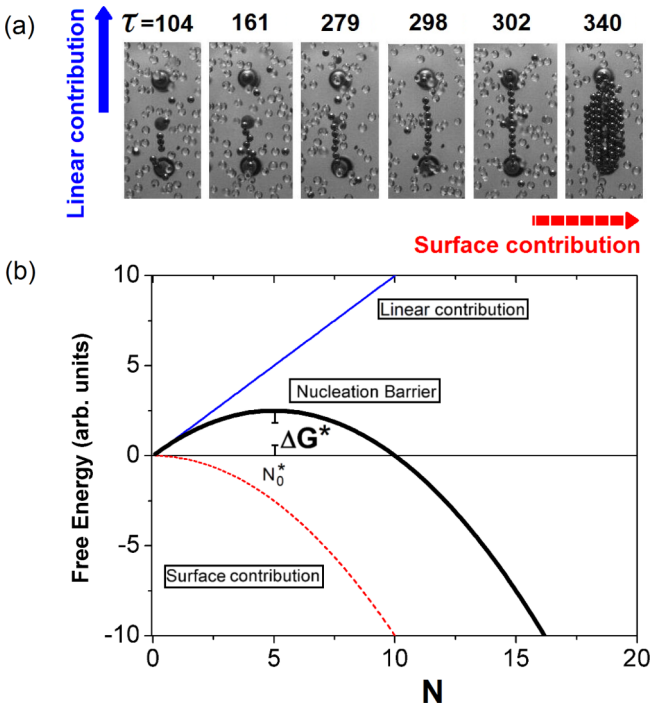

FIG. 2. (Color online) (a) A sequence of photographs showing the nucleation process. A chain must form before the aggregation begins. In this example, $\Gamma = 2.9$ and $\phi = 0.05$. Time is measured in seconds. Note the large time elapsed for the chain to form compared to the time it takes a further aggregation. (b) The change in free energy as a function of the number of paramagnetic beads in the cluster, N. N_0^* is the critical size of the nucleus and ΔG^* is the nucleation barrier.

one hand, there is a positive linear contribution to form the primary chain (proportional to N, where N is the number of beads) and a negative one that grows quadratically to increase the area of the cluster (proportional to N^2); see Fig. 2(b). The signs are justified if we recall that in the first case (the growth of the chain) there are unsaturated bonds while in the second, the bonds in the "bulk" are saturated. Exactly as in molecular nucleation. Then, one can write the following expression for the free-energy change: $\Delta G \propto N - \frac{N^2}{10}$. The denominator in the second term is introduced to constrain the cluster to the size of the seed. Accordingly, at $N = N_0^* = 5$ ($\Delta G = \Delta G^*$) the quadratic term starts to dominate and ΔG has an inflection point. The cluster starts to be stable only when $\Delta G = 0$ ($N = 10$).

In molecular and mesoscopic systems it is hard to describe the nucleation stage and the temporal evolution of the aggregation. Indeed, three time scales are always needed [35]. In our case it is much easier. We can define the nucleation time τ as the time in which the primary chain (the chain that links the dipoles) completely forms. Let us remark that in this stage small chains can form (for example, as lengthy as $N = 3$) but quickly disintegrate because ΔG is still positive. τ is measured starting right after the seed is put on its position (both dipoles) until the formation of a full chain connecting the magnetic points; see Fig. 2(a). Phenomenologically, we found that τ as a function of Γ exhibits a power-law behavior and diverges at $\Gamma^* = 3$ (see Fig. 3). Note that the denser the

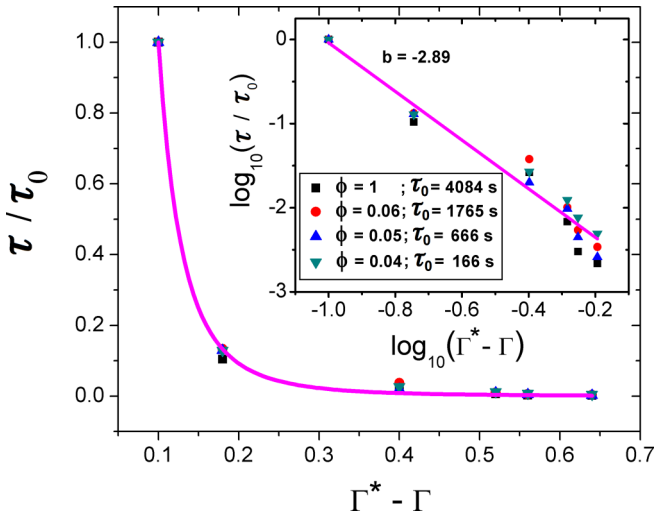

FIG. 3. (Color online) The nucleation time as a function of $\Gamma^* - \Gamma$, where $\Gamma^* = 3$, for four different values of ϕ (where $n_p = 89$). Inset: the straight line shows that the nucleation time follows a power law with $\Gamma^* - \Gamma$. b is the slope of the line. τ_0 is the time at which the formation of the primary chain occurs at $\Gamma = 2.9$. Clearly, τ_0 varies with ϕ.

bath is (in this case, low ϕ), the lower the nucleation time. This is because energy injected to the system is reduced by dissipation and, thus, the nucleation is driven mostly by the magnetic interaction. The opposite happens, however, for the case of a dilute gas (where the inertial forces dominate).

What we observe in the high-speed camera films during the aggregation process can be qualitatively described as follows: when a paramagnetic particle passes near to the primary chain, a dipolar magnetic moment is induced on it. They interact and the bead can be trapped in a local minimum of energy. This lateral aggregation repeats until the cluster reaches its maximum size. Due to the finite size and interaction of the magnetic beads, as the aggregate increases, the magnetic interaction intensity decreases. Then, the maximum size of the cluster is reached when the magnetic interaction becomes too weak to counteract the drift effect due to collisions with glass particles and the inertial effects due to the vibrations. Similar observations have been reported in other magnetic systems [27,28,31,32]. During the aggregation process some branches may grow [see Figs. 4(a)–4(f)]. It occurs some times that, when two branches connect to each other, an excluded area or void is generated. Then some glass particles can fall in this reduced region. Due to the collisions with the borders of the void, these particles lose kinetic energy and remain dynamically arrested.

Since the clusters studied in this work are 2D structures immersed in a thermal bath, at the early stages of the aggregation process the whole structure evolves in time. However, after a characteristic time, the cluster reaches a stable configuration. This is what we call the final structure of the cluster. Bear in mind that the final structure is not unique but varies at each experiment. This is because there are large fluctuations and the strong competition between inertial and magnetic forces generates a chaotic dynamics. One can observe in the photographs that the final structure of the

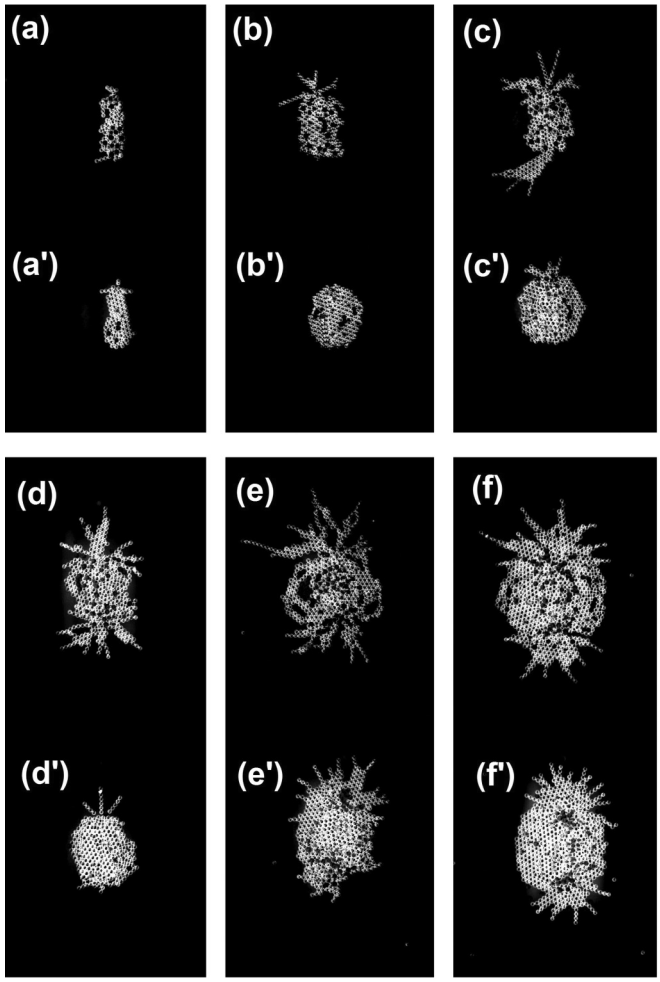

FIG. 4. Photographs (a)–(f) show the final structures of the aggregates. Here, $\Gamma = 2.56$ and $\phi = 0.105, 0.211, 0.317, 0.428, 0.6$, and 0.84, respectively, where $n_g = 952$. Photographs (a′)–(f′) show the corresponding final structure of the clusters after an annealing process produced by changing Γ in steps of $\Delta\Gamma = 0.03$, sustaining each acceleration during a time interval of $t = 10s$.

clusters has, in general, disordered (vitreous) characteristics, containing some impurities (glass particles). Figures 4(a)–4(f) show the structures obtained for different values of Γ and ϕ. Empirically, we have found that 5 min of vibration with no structural changes in a cluster is enough to claim that such cluster is in a stable configuration.

IV. ANNEALING

One of the simplest ways to generate a glass is by supercooling a liquid. When the molecules in a liquid lose their capability to explore their entire phase space due to a sudden cooling process, they become trapped in a local minimum of free energy. Under these conditions the liquid transforms into a nonordered solid structure that emerges as a consequence of the large number of molecules trapped in metastable states. There, the system exhibits a very slow dynamics. We can anneal such disordered structures if the system is heated up, close to the melting point. Once the molecules recover the capability to access the phase space, the system is cooled

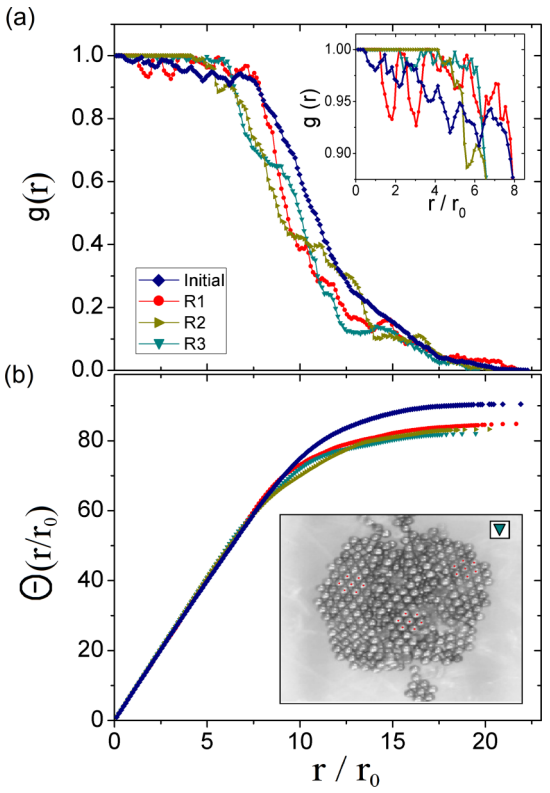

FIG. 5. (Color online) (a) Shows the radial distribution functions of the final structure obtained by the clusters exposed to heating-cooling processes with different ramps ($R1$, $R2$, and $R3$) where $\Delta\Gamma$ =0.34, 0.11, and 0.03 with time intervals from 10 to 30 s. The inset shows a zoom of the lines for short r. (b) Shows the compaction changes in these 2D structures in terms of the surface integral of the mass radial distribution. The inset shows a zoom of the annealed structure depicted in Fig. 4(d′).

slowly in order to reach a deeper minimum of energy. By repeating this procedure, a crystalline structure is obtained.

Now we discuss how this annealing phenomenon can be reproduced in our system. Taking a disordered cluster, we increase Γ following a given ramp to reach a maximum granular temperature and then return to its initial value. We set different ramps with ($\Delta\Gamma = 0.03$–0.34 and $\Delta t = 10$–30 s).

What we observe is that for most of the ramps, the final structure obtained after the first heating-cooling cycle is more compact. Furthermore, when the cooling rate is slow enough, the compaction degree and order attained in the structure are higher, see Figs. 4(a′)–4(f′) [see in the inset of Fig. 5(b) a zoom of the image depicted in Fig. 4(d′)]. For large cooling rates, disordered structures are always obtained. Indeed, we have found that, for any ϕ, it is enough to impose a cooling rate of $\Delta\Gamma$ =0.03 every 10 s to obtain an ordered structure.

To characterize and quantify the attained degree of order, we calculate the radial distribution of mass. For 2D objects this quantity is given by the following expression:

$$g(r) = \frac{M(r+\Delta) - M(r)}{\pi[(r+\Delta)^2 - r^2]}, \qquad (2)$$

where $M(r)$ is the mass contained in a circle of radius r and Δ is a small increment in r. This radial distribution for our clusters was obtained from high resolution digital pictures making a high-contrast treatment.

Figure 5(a) shows the radial distribution function of the structures obtained after three annealing cycles with different Γ ramps. Clearly, after the annealing cycles, the clusters become more compact. When the annealing is slow ($R3$), a close-packed structure with hexagonal patches is clearly observed [see the inset of Fig. 5(b)], where it is clear that $g(r)$ flattens for small values of r (in other words, corrals or voids, responsible for the fluctuations, disappear). An average compaction coefficient, Θ, can be calculated directly by integrating $g(r)$. Figure 5(b) shows the evolution of $\Theta(r/r_0)$ with the annealing cycles. Here, r_0 is the particle diameter. The upper curve shows $\Theta(r/r_0)$ before the annealing and the other curves show after the annealing with different ramps.

In order to quantify the structural changes generated by the annealing, it is convenient to evaluate the evolution of the lacunarity index F_λ. This quantity is used to evaluate some characteristics of the pixel distribution, and statistically describes not only the local occupancy factor, but how the lacunae and inhomogeneities occur at different scales in the structure. It might also capture some information related to the main symmetries of the interactions responsible of the aggregation. In this sense, the lacunarity index has been used to describe landscape textures. In order to find this index, we follow the next steps: (i) we draw ten sets of concentric boxes of relative size ϵ that changes exponentially, at different sites of the structure ($\epsilon = 1$ means that the whole structure fits inside a box), (ii) we measure the number of pixels inside boxes of equal sizes, and (iii) we calculate $F_\lambda = (\sigma/\mu)^2$, where σ and μ are, respectively, the standard deviation and the average number of the pixel distributions.

Figure 6 shows F_λ obtained from a structure at two different times of the annealing process. Clearly, if $Ln(\epsilon) < Ln(\epsilon_0)$ (scales shorter than r_0) the corresponding values of F_λ increase; after that (scales larger than r_0) the values of the lacunarity index reduce and even more when the border of the structure is reached.

We now evaluate the correlations coexisting in the structures during the annealing process. In particular, we

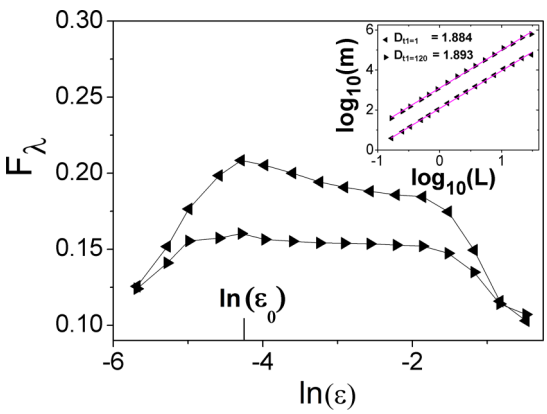

FIG. 6. (Color online) F_λ vs. ϵ for the clusters of Fig. 7(c) at $t_1 = 1$ and 120 s. Inset: Log-log graph of the average number of pixels (m) versus L for such clusters. The slopes of the fitted straight lines are the corresponding mass fractal dimensions. The lines were separated by a constant to appreciate their differences.

characterize the complexity of some structures by considering the mass fractal dimension. This quantity can be defined by means of the following power law $m \propto L^D$, where m is the mass contained in square boxes of lateral size L. Providing this power law fits well the experimental measurements, D is the mass fractal dimension of this 2D object. The practical procedure to determine D is as follows: we draw a number of equally separated concentric square boxes of side L centered at a given site. The number of pixels contained in the boxes is proportional to the mass. This procedure is repeated for several different sites of the digital picture. Then, we average the number of pixels for boxes of the same size. This allows us to avoid the effects of small local inhomogeneities and makes it possible to capture the statistical correlations of the structure [36]. D is the slope of the resulting straight line fitting the experimental data (see inset of Fig. 6).

To follow the evolution of the structures [for example, the one in Fig. 4(d)] under the annealing process, we plot a mean value of F_λ (Λ) and the mass fractal dimension D, as a function of Γ, for four heating-cooling cycles; see Fig. 7. In the first cycle, we can observe the strongest change in the area of the structure (black squares in the inset). Note that the area oscillates. This is because upon heating the system (i.e., when Γ is increased), the area of the cluster diminishes, and when cooling, it slightly augments. The envelope follows the crests of these oscillations. We found empirically that four cycles are sufficient to obtain a small amplitude in the oscillations. The annealing reduces the number of lacunae because the particles reaccommodate themselves, relaxing into deeper free-energy minima. In these physical conditions a crystalline-like structure forms; see Fig. 7(c).

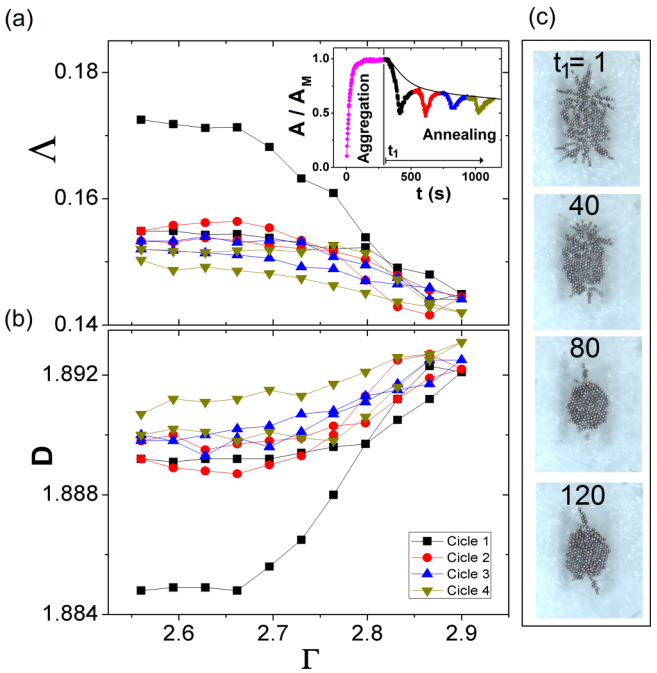

FIG. 7. (Color online) (a) Shows the evolution of the lacunarity index of the cluster in Fig. 4(d), in Fig. 4, from $\Gamma = 2.56$ to $\Gamma = 2.9$, with a change of $\Delta\Gamma = 0.03$ each 10 s. Note that in each cycle Λ decreases. The inset shows the change in the area of the cluster. The initial increasing part of the curve shown with magenta diamonds corresponds to the moments of aggregation. (b) The corresponding evolution of the fractal dimension D after four annealing cycles. Note that in each cycle D increases. (c) The cluster structure at four times (in seconds) during the first annealing cycle.

Disintegration

Finally, we explore the physical situation when disintegration occurs. How fast this event occurs depends on several factors: obviously, the concentration of magnetic and glass particles (ϕ) and the strength of magnetic moment of the seed and particles. For the sake of simplicity, we conduct experiments under the following conditions: we start with a formed cluster for a given value of ϕ, then suddenly we remove the magnetic dipoles and follow the process of disintegration. As expected, the general trend we observed is a diffusive flow from the region occupied by the cluster toward the periphery, which roughly resembles the diffusive process of an ink droplet put into water [37] [see Fig. 8(a)]. To describe the kinetics of the disintegration of the clusters under these conditions let us define C as the concentration of particles in a given area and time. C has its maximum value C_0 just before the field (both spherical dipoles) is removed (we call this time $t = 0$). Thereafter, the concentration decreases to reach a basal value C_f, which is the number of paramagnetic particles when they are homogeneously distributed in the whole cell. A reasonable supposition is that the time rate of the disintegration is proportional to $C - C_f$,

$$\frac{dC}{dt} = -k(C - C_f), \tag{3}$$

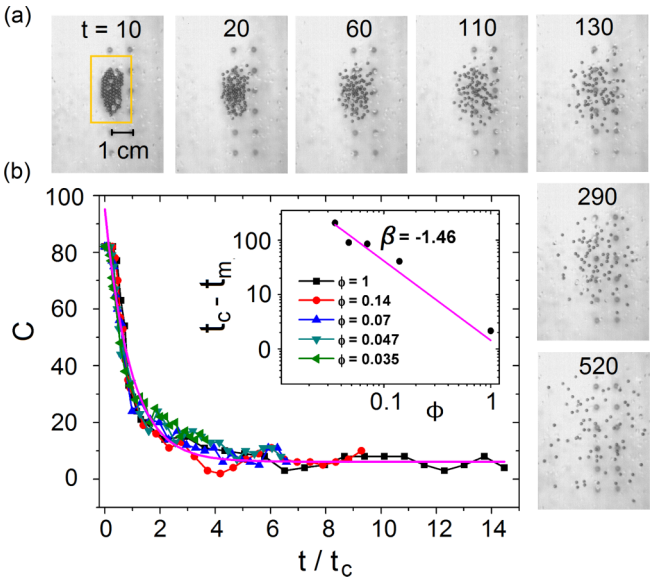

FIG. 8. (Color online) (a) A sequence of snapshots to illustrate the disintegration of a granular cluster at $\Gamma = 2.9$ and $\phi = 0.047$ (for $n_p = 89$). Time is measured in milliseconds. (b) C as a function of time for $\Gamma = 2.9$ and five relative concentrations $\phi = 0.035$, 0.047, 0.07, 0.14, and 1. C is the concentration of beads inside the yellow box at a given time. The solid line is the best fit for $\phi = 1$. The curves collapse when time is normalized to t_c. We plot in the inset $t_c - t_m$ vs. ϕ; see the text for details.

where $1/k$ is a characteristic time t_c at which C_0 diminishes by a $1/e$ factor. This rate equation has a simple solution:

$$C = C_f + (C_0 - C_f)\exp^{(-kt)}. \quad (4)$$

The measured concentrations for various values of ϕ (0.035, 0.047, 0.07, 0.14, 1) are shown in Fig. 8(b). The solid line is the best fit obtained using equation 4 for $\phi = 1$. Interestingly, as ϕ decreases (i.e., n_g increases), t_c increases. This is due to the fact that the metallic beads diffuse out of the region formerly occupied by the cluster through a denser medium of glass beads. The inset of Fig. 8(b) confirms this. Indeed, the power law $t_c = t_m + \alpha\phi^\beta$ (where t_m, α, and β are fitting parameters whose values are 67, 1.42, and 1.46 ms, respectively) implies that if ϕ is very small t_c diverges, and if it is very high (for example, only one glass bead in the cell) the second term is null and t_c is close to t_m. In other words, t_m is the minimum time the cluster will take to disintegrate in "vacuum" (at a given Γ). In future work we will investigate how the above parameters depend on Γ.

V. CONCLUSIONS

The processes of nucleation, aggregation, annealing, and disintegration in a driven granular system, composed by paramagnetic beads immersed in a thermal bath of glass beads, are studied. We learned that, during the accretion, the nucleation and aggregation are well-differentiated processes. As far as we know, this is the first time that a nucleation process has been experimentally studied in a macroscopic system formed by interacting beads. Based on the analogy with the annealing of a molecular glass, and on some quantitative measures of the complexity of the structure of the aggregates (mass distribution function, lacunarity index, and fractal dimension), the annealing of a granular aggregate was quantified and discussed in detail. This helped us to also learn that, in spite of the anisotropy of the magnetic potential, the annealing induces structural rearrangements where hexagonal patches are observed. Finally, we found that upon removing the external magnetic field, the clusters disintegrate through the surrounding granular gas with a characteristic exponential decay that depends on ϕ.

ACKNOWLEDGMENTS

This work has been supported by Conacyt, Mexico, under Grants No. 101384 and No. 104616, and VIEP-BUAP Grant No. CAEJ-EXC13-3. J.G.G. acknowledges support through a fellowship from CONACyT.

[1] M. O. Andreae, Science **339**, 911 (2013).
[2] U. Gasser, E. R. Weeks, A. Schofield, P. N. Pusey, and D. A. Weitz, Science **292**, 258 (2001).
[3] H. Kasumi, Y. E. Solomentsev, S. A. Guelcher, J. L. Anderson, and P. J. Sides, J. Colloid Interface Sci. **232**, 111 (2000).
[4] S. J. Veen, O. Antoniuk, B. Weber, M. A. C. Potenza, S. Mazzoni, P. Schall, and G. H. Wegdam, Phys. Rev. Lett. **109**, 248302 (2012).
[5] B. J. Reynwar, G. Illya, V. A. Harmandaris, M. M. Muller, K. Kremer, and M. Deserno, Nature **447**, 461 (2007).
[6] D. J. Scheeres, C. M. Hartzell, P. Sánchez, and M. Swift, Icarus **210**, 968 (2010).
[7] T. C. Halsey, M. H. Jensen, L. P. Kadanoff, I. Procaccia, and B. I. Shraiman, Phys. Rev. A **33**, 1141 (1986).
[8] T. C. Halsey, B. Duplantier, and K. Honda, Phys. Rev. Lett. **78**, 1719 (1997).
[9] P. Meakin, Phys. Rev. B **28**, 5221 (1983).
[10] T. Nagatani, Phys. Rev. A **37**, 3514 (1988); **39**, 438 (1989).
[11] B. B. Mandelbrot, *Fractals in Biology and Medicine*, Mathematics and Biosciences in Interaction (Birkhauser, Basel, 1994).
[12] B. B. Mandelbrot, H. Kaufman, A. Vespignani, I. Yekutieli, and C. H. Lam, Europhys. Lett. **29**, 599 (1995).
[13] B. B. Mandelbrot, B. Kol, and A. Aharony, Phys. Rev. Lett. **88**, 055501 (2002).
[14] M. Ausloos, N. Vandewalle, and R. Cloots, Europhys. Lett. **24**, 629 (1993).
[15] A. Inoue and J. S. Gook, Mater. Trans., JIM **36**, 1180 (1995).
[16] A. Inoue, T. Zhang, T. Itoi, and A. Takeuchi, Mater. Trans., JIM **38**, 359 (1997).
[17] R. Moctezuma, M. E. Mendoza, and J. L. Carrillo, J. Magn. Magn. Mat. **320**, e186 (2008).
[18] D. L. Stein and C. M. Newman, *Spin Glasses and Complexity* (Princeton University Press, Princeton, NJ, 2013).
[19] T. J. Sluckin, D. A. Dunmur, and H. Stegemeyer, *Crystals That Flow* (Taylor and Francis, London, UK, 2004).
[20] E. M. de la Calleja Mora, J. L. Carrillo, M. E. Mendoza, and F. Donado, Eur. Phys. J. B **86**, 126 (2013).
[21] Y. Nahmad-Molinari and J. C. Ruiz-Suárez, Phys. Rev. Lett. **89**, 264302 (2002).
[22] A. Panaitescu, K. A. Reddy, and A. Kudrolli, Phys. Rev. Lett. **108**, 108001 (2012).
[23] A. Kudrolli, M. Wolpert, and J. P. Gollub, Phys. Rev. Lett. **78**, 1383 (1997).
[24] P. Melby, A. Prevost, D. A. Egolf, and J. S. Urbach, Phys. Rev. E **76**, 051307 (2007).
[25] S. Dorbolo, M. Brandenbourger, F. Damanet, H. Dister, F. Ludewig, D. Terwagne, G. Lumay, and N. Vandewalle, Eur. J. Phys. **32**, 1465 (2011).
[26] O. Carvente and J. C. Ruiz-Suarez, Phys. Rev. Lett. **95**, 018001 (2005).
[27] D. L. Blair and A. Kudrolli, Phys. Rev. E **67**, 021302 (2003).
[28] A. Snezhko, I. S. Aranson, and W.-K. Kwok, Phys. Rev. Lett. **94**, 108002 (2005).
[29] O. Carvente and J. C. Ruiz-Suárez, Phys. Rev. E **78**, 011302 (2008).
[30] O. Carvente, G. G. Peraza-Mues, J. M. Salazar, and J. C. Ruiz-Suárez, Granular Matter **14**, 303 (2012).
[31] J. Gonzalez-Gutierrez, J. L. Carrillo-Estrada, and J. C. Ruiz-Suarez, J. Stat. Mech. (2013) P12015.

[32] J. Gonzalez-Gutierrez, J. L. Carrillo-Estrada, and J. C. Ruiz-Suarez, J. Phys.: Conf. Ser. **475**, 012003 (2013).
[33] P. M. Reis, R. A. Ingale, and M. D. Shattuck, Phys. Rev. E **75**, 051311 (2007).
[34] J. S. Olafsen and J. S. Urbach, Phys. Rev. E **60**, R2468 (1999).
[35] J. M. Garcia-Ruiz, J. Struct. Biol. **142**, 22 (2003).
[36] J. L. Carrillo, F. Donado, and M. E. Mendoza, Phys. Rev. E **68**, 061509 (2003).
[37] S. Lee, H. Y. Lee, I. F. Lee, and C. Y. Tseng, Eur. J. Phys. **25**, 331 (2004).